

## Heavy quark diffusion with relativistic Langevin dynamics in the quark-gluon fluid

Yukinao Akamatsu, Tetsuo Hatsuda, and Tetsufumi Hirano

*Department of Physics, The University of Tokyo, Tokyo 113-0033, Japan*

(Received 25 September 2008; published 11 May 2009)

The relativistic diffusion process of heavy quarks is formulated on the basis of the relativistic Langevin equation in Itô discretization scheme. The drag force inside the quark-gluon plasma (QGP) is parametrized according to the formula for the strongly coupled plasma obtained by the anti-de-Sitter space/conformal field theory (AdS/CFT) correspondence. The diffusion dynamics of charm and bottom quarks in QGP is described by combining the Langevin simulation under the background matter described by the relativistic hydrodynamics. Theoretical calculations of the nuclear modification factor  $R_{AA}$  and the elliptic flow  $v_2$  for the single electrons from the charm and bottom decays are compared with the experimental data from the relativistic heavy-ion collisions. The  $R_{AA}$  for electrons with large transverse momentum ( $p_T > 3$  GeV) indicates that the drag force from the QGP is as strong as the AdS/CFT prediction.

DOI: [10.1103/PhysRevC.79.054907](https://doi.org/10.1103/PhysRevC.79.054907)

PACS number(s): 24.85.+p, 05.40.Jc, 11.25.Tq, 25.75.-q

### I. INTRODUCTION

The physics of the quark-gluon plasma (QGP) is actively studied by means of the relativistic heavy-ion collisions at Relativistic Heavy Ion Collider (RHIC) in BNL and will be pursued further at Large Hadron Collider (LHC) in CERN [1]. The space-time evolution of the heavy-ion collisions at RHIC is well described by the (3+1)-dimensional relativistic hydrodynamics supplemented with the hadronic cascade after chemical freeze-out [2]. Information on the collective dynamics of QGP is obtained by the soft probes such as distributions of light hadrons at low momentum, while the information of microscopic dynamics of QGP is obtained by the hard probes such as jets, heavy quarks, and heavy quarkoniums [3].

In the present article, we focus on charm and bottom quarks that behave as impurities in QGP. Experimentally, the signal of the heavy quarks can be extracted from the single electron spectra through semileptonic decays [4,5]. Theoretically, the energy loss of heavy quarks in QGP has been estimated in perturbative QCD (pQCD) techniques [6,7]. However, it was pointed out recently that the convergence of the weak coupling expansion of the drag force for heavy quarks is rather poor at the temperature relevant to RHIC and LHC so the calculation in the leading order would not be reliable [8]. Possible alternative way to estimate the drag force is to use the duality conjecture between the gauge theory and string theory [anti-de-Sitter space/conformal field theory (AdS/CFT) correspondence] [9–11]. Although it can be applied only to the  $\mathcal{N} = 4$  supersymmetric Yang-Mills plasma with large 't Hooft coupling, the result obtained may provide us with a hint for the drag force in the strong coupling regime of the quantum chromodynamics (QCD) plasma if appropriate translation is made [12].

The purpose of this article is to study the connection between the drag force acting on the charm and bottom quarks in QGP and the final electron spectra. To make such connection, we introduce relativistic Langevin equation for heavy quarks under the background of the quark-gluon fluid

described by the ideal hydrodynamics. We need relativity because the transverse momentum of the heavy quarks at RHIC is not necessarily smaller than their rest masses. Our relativistic Langevin equation is formulated in Itô discretization scheme. The diffusion constant and the drag force are related through a generalized fluctuation-dissipation relation. As for the drag force, two distinct models, perturbative QCD (pQCD) and AdS/CFT, are considered. To calculate the space-time dynamics of light quarks and gluons, (3+1)-dimensional hydrodynamics is used, which is necessary to calculate the electron spectra of different impact parameters in the heavy-ion collisions. The Langevin equation for heavy quarks is numerically solved from the initial distribution generated by Monte Carlo generator PYTHIA [13] until the freeze-out of the heavy quarks. The transverse-momentum ( $p_T$ ) dependence of the nuclear modification factor ( $R_{AA}$ ) and the elliptic flow ( $v_2$ ) of single electrons as decay products of heavy quarks are calculated and compared with the RHIC data.

This article is organized as follows. In Sec. II, after formulating the relativistic Langevin equation and a generalized fluctuation-dissipation relation, we introduce two extreme models of the drag force motivated by pQCD and AdS/CFT. In Sec. III, the relativistic hydrodynamics for light degrees of freedom and the relativistic Langevin equation for heavy degrees of freedom are combined to describe the heavy quark diffusion in dynamical QGP fluid. The initial condition of heavy quarks, the algorithm of Langevin simulation in dynamical background, and the treatment of the freeze-out and decay of heavy quarks are discussed in detail. In Sec. IV, the numerical results of our calculation are presented. We show the profile of heavy quark diffusion, heavy quark spectra, and single-electron spectra and compare our single-electron spectra with experimental data. Physical meaning of our results are also discussed. Section V is devoted to summary and concluding remarks. In Appendix, we show a derivation of the relativistic Kramers equation from the relativistic Langevin equation in the Itô discretization scheme.

## II. LANGEVIN DYNAMICS OF HEAVY QUARKS

In this section, we formulate the relativistic Langevin equation in the local rest frame of the fluid. A generalized form of the fluctuation-dissipation relation is derived. Then, we discuss the drag forces calculated in the pQCD approach and in the AdS/CFT approach. Finally, we introduce a phenomenological model of the drag coefficient  $\Gamma$  and the diffusion constant  $D$  that satisfy the generalized fluctuation-dissipation relation.

### A. Relativistic Brownian motion

Suppose that there exist a time scale  $\tau_B$  during which a Brownian particle changes its momentum and a microscopic time scale  $\tau_m$  during which light dynamical degrees of freedom change state and lose time correlation. If these time scales satisfy  $\tau_B \gg \tau_m$ , one can describe the Brownian particle by the Langevin equation [14]. In such a situation that the charm/bottom diffuses inside the quark-gluon plasma, there are some extra complications: (i) The background quark-gluon fluid expands rapidly in space and time with the local 4-velocity  $u^\mu(\vec{x}, t)$  and (ii) the initial momentum distribution of the charm/bottom governed by the hard QCD process has high momentum component larger than their quark masses.

As for (i), we define the Langevin equation in the rest frame of matter [ $u^\mu = (1, 0, 0, 0)$ ] and the real motion of the Brownian particle is obtained by the local Lorentz boost back to the moving frame. As for (ii), we take into account the relativistic kinematics of the Brownian particle in a minimal way by using relativistic dispersion relation  $E(p) = \sqrt{p^2 + M^2}$ . Then the Langevin equation in the rest frame of matter with minimum relativistic kinematics may be written as [15]

$$\Delta \vec{x}(t) = \frac{\vec{p}}{E(p)} \Delta t, \quad (1)$$

$$\Delta \vec{p}(t) = -\Gamma(p) \vec{p} \Delta t + \vec{\xi}(t). \quad (2)$$

Here  $\Delta \vec{x}(t) = \vec{x}(t') - \vec{x}(t)$  and  $\Delta \vec{p}(t) = \vec{p}(t') - \vec{p}(t)$  and  $\Delta t \equiv t' - t$  is a discrete step of time. The momentum-dependent drag coefficient is denoted by  $\Gamma(p)$  that is related to the time scale of the Brownian particle  $\tau_B \sim \Gamma^{-1}$ . Also  $\vec{\xi}(t)$  is a noise obeying the probability distribution  $W[\vec{\xi}(t)]$  that we take to be the Gaussian white noise with a normalization constant  $C$ :

$$W[\vec{\xi}(t)] d^3 \xi(t) = C \exp \left[ -\frac{\vec{\xi}(t)^2}{2D(p)\Delta t} \right] d^3 \xi(t). \quad (3)$$

This leads to

$$\langle \xi_i(t) \rangle = 0, \quad (4)$$

$$\langle \xi_i(t) \xi_j(t') \rangle = D(p) \delta_{ij} \delta_{tt'} \Delta t, \quad (5)$$

where  $D(p)$  is a momentum-dependent diffusion constant. Note that  $\xi(t)$  is not a single microscopic kick but a sum of microscopic kicks during the time  $\Delta t$ .

Throughout this article, we use the Itô discretization scheme of the Langevin equation; namely all the argument of  $\vec{p}$  in the right-hand side of Eqs. (1) and (2) are evaluated at the prepoint time  $t$ . This is particularly useful for numerical simulations due

to obvious reason. The relativistic Kramers equation, which is a partial differential equation for the probability of the particle distribution in the phase space  $P(\vec{p}, \vec{x}, t)$ , is then obtained as (see the derivation in Appendix)

$$\begin{aligned} & \left( \frac{\partial}{\partial t} + \frac{\vec{p}}{E} \frac{\partial}{\partial \vec{x}} \right) P(\vec{p}, \vec{x}, t) \\ &= \frac{\partial}{\partial \vec{p}} \left[ \Gamma(p) \vec{p} + \frac{1}{2} \frac{\partial}{\partial \vec{p}} D(p) \right] P(\vec{p}, \vec{x}, t). \end{aligned} \quad (6)$$

Note that  $\partial/\partial \vec{p}$  acts not only on  $P$  but also on  $\Gamma(p)$  and  $D(p)$ .

Demanding that Eq. (6) has the relativistic Maxwell-Boltzmann distribution (the Jüttner distribution)  $P(\vec{p}, \vec{x}, t) \propto \exp[-\sqrt{p^2 + M^2}/T]$  as a stationary solution, we obtain a constraint between the drag and the diffusion as

$$\Gamma(p) + G(p) = \frac{D(p)}{2ET}, \quad (7)$$

with  $G(p) \equiv dD(p)/2pdp = dD(p)/d(p^2)$ . If  $D$  is  $p$ -independent, Eq. (7) reduces to the relativistic analog of the Einstein relation  $\Gamma = \frac{D}{2ET} = \frac{M}{E} \frac{D}{2MT}$  obtained in Ref. [15].

### B. Modeling the energy loss of heavy quarks

Energy loss of heavy quarks in the deconfined phase has two sources; the collisional energy loss due to elastic scattering of a heavy quark with the plasma constituents and the radiative energy loss associated with the induced emission of the gluon. In the leading order (LO) of the weak-coupling QCD perturbation, these processes are found to have different momentum dependence of the heavy quark and could become comparable in magnitude [6,7]. Recently, the convergence of such weak-coupling expansion was questioned by an explicit calculation of the collisional process in the next-to-leading order (NLO) [8]: The drag coefficient for the three-color, three-flavor QCD in the nonrelativistic kinematics ( $M \gg T, p$ ) reads

$$\Gamma_{\text{pQCD}}|_{M \gg T, p} \simeq \frac{8\pi}{3} \alpha_s^2 \frac{T^2}{M} (-\ln g + 0.07428 + 1.8869g). \quad (8)$$

For the QCD coupling constant relevant at RHIC and LHC ( $g \sim 2$ ), the weak-coupling expansion has an obvious problem of convergence. From the phenomenological point of view, it has been argued in the past that relatively large drag force is necessary to account for the RHIC data [16,17].

Alternative approach to the drag force is provided by the AdS/CFT correspondence [9–11]. In the  $\mathcal{N} = 4$  super-Yang-Mills theory (SYM) at large  $N_c$  and large 't Hooft coupling  $\lambda \equiv g_{\text{SYM}}^2 N_c$ , energy loss of an external quark with velocity  $v$  is obtained as

$$\frac{dp}{dt} = -\frac{\pi\sqrt{\lambda}}{2} T_{\text{SYM}}^2 \frac{v}{\sqrt{1-v^2}} \quad (9)$$

$$\simeq -\frac{\pi\sqrt{\lambda}}{2} T_{\text{SYM}}^2 \frac{p}{M}. \quad (10)$$

Here the first equation is valid for arbitrary mass of external quark, while the second equation is valid for  $M \gg \sqrt{\lambda} T$  [11].

By matching the energy density and the heavy quark potential in the SYM plasma to those in QCD plasma, one finds  $T_{\text{SYM}} \simeq T_{\text{QCD}}/3^{1/4}$  and  $3.5 \leq \lambda \leq 8.0$  [12]. Then, the drag coefficients may be estimated as

$$\Gamma_{\text{AdS/CFT}} = (2.1 \pm 0.5) \frac{T^2}{M}. \quad (11)$$

A remarkable feature of this formula in contrast to the weak-coupling estimate is that  $\Gamma$  is  $p$  independent [11]. The fundamental question here is, of course, the reliability of the translation from SYM to QCD both conceptually and numerically.

Given the theoretical uncertainties in estimating the drag force as mentioned above, we will take a phenomenological approach in this article: We adopt the parametric dependence of the drag coefficient motivated by the AdS/CFT in Eq. (11) with the overall magnitude left as a free parameter:

$$\Gamma \equiv \gamma \frac{T^2}{M}. \quad (12)$$

The dimensionless drag coefficient  $\gamma$  is assumed to be independent of  $T$ ,  $M$ , and  $p$  throughout this article. The corresponding diffusion constant  $D$  is obtained from the generalized fluctuation-dissipation relation in Eq. (7) with the physical boundary condition,  $D \rightarrow 0$  as  $\Gamma \rightarrow 0$ :

$$D = 2ET \cdot \Gamma \cdot \left(1 + \frac{T}{E}\right) = \gamma \frac{2T^3}{M} (E + T). \quad (13)$$

It is in order here to make two remarks on the dynamics we employed in Eqs. (12) and (13). (i) Because we have assumed  $\Gamma$  to be  $p$ -independent motivated by AdS/CFT, the diffusion constant  $D$  depends necessarily on the momentum of the Brownian particle. One may alternatively assume that  $D$  is independent of  $p$  while  $\Gamma$  depends on  $p$  as  $\Gamma(p) = D/[2E(p)T]$  [15]. Such dynamics would simulate the  $p$  dependence of the drag force due to collisional process in the weak-coupling regime [7]. (ii) At ultrahigh energies  $p \gg M$ , the dominant energy loss occurs through the induced emission of the gluons. In this case, the condition  $\tau_B \gg \tau_m$  is violated. Thus the Langevin approach becomes inapplicable [11] and a different approach based on radiative energy loss is required to describe heavy quarks in the QGP [7,18]. With these reservations in mind, we consider our ansatz Eqs. (12) and (13) as phenomenological but characteristic dynamics of QCD and try to estimate  $\gamma$  from the observed single electron data at RHIC in later sections.

### III. HYDRO + HEAVY-QUARK MODEL

#### A. Background QGP fluid

The hydrodynamics has been quite successful in the description of collective flow phenomena in heavy-ion collisions at RHIC. Because the hydrodynamics gives space-time evolution of temperature and flow velocity of the fluid so that the local rest frame of fluid is well-defined. Then, the Langevin equation in the previous section formulated in the local rest frame of the fluid is applicable directly.

Let us first summarize the relativistic hydrodynamic model [2,19–21] whose basic equation reads

$$\partial_\mu T^{\mu\nu} = 0. \quad (14)$$

Here  $T^{\mu\nu}$  is energy-momentum tensor. For strongly interacting matter with zero viscosity,  $T^{\mu\nu}$  becomes

$$T^{\mu\nu} = (e + P)u^\mu u^\nu - P g^{\mu\nu}, \quad (15)$$

where  $e$ ,  $P$ , and  $u^\mu$  are energy density, pressure, and four fluid velocity, respectively. The baryon chemical potential is neglected, because it is small near midrapidity at RHIC energies. We solve Eq. (14) in the Bjorken coordinates  $(\tau, x, y, \eta_s)$ , where  $\tau = \sqrt{t^2 - z^2}$  and  $\eta_s = \frac{1}{2} \ln[(t+z)/(t-z)]$  are proper time and space-time rapidity, respectively.

In the high temperature ( $T > T_c = 170$  MeV) QGP phase, we employ the bag equation of state (EOS) for massless partons ( $u, d, s$  quarks and gluons) with  $B^{1/4} = 247.19$  MeV. Here the bag constant is tuned to have transition to the hadron resonance gas at  $T_c$ . In the hadron phase ( $T < T_c = 170$  MeV), a resonance gas of hadrons with the mass up to  $\Delta(1232)$  is employed [21]. Volume fraction of QGP  $f_{\text{QGP}}$  in the mixed phase is

$$f_{\text{QGP}} = \frac{e - e_{\text{had}}}{e_{\text{QGP}} - e_{\text{had}}}, \quad (16)$$

where  $e_{\text{QGP}}$  ( $e_{\text{had}}$ ) is the maximum (minimum) value of the energy density in the mixed phase [22]. Later we will utilize  $f_{\text{QGP}}$  to define the effective lifetime of QGP and the freezeout condition for the heavy quarks.

Hot QGP with local thermalization is assumed to be produced at  $\tau_0 = 0.6$  fm. The entropy density distribution at  $\tau_0$  in the midrapidity is taken to be proportional to a linear combination of the number densities of participants and binary collisions in the transverse plane [19]. For the initial condition of the flow velocity, Bjorken's scaling solution,  $u_x(\tau_0) = u_y(\tau_0) = 0$  and  $u_z(\tau_0) = \sinh \eta_s$ , is employed [24]. With these initial conditions, the hydrodynamic model can well reproduce the experimental data of charged particles at RHIC [2].

The space-time evolution of the QGP fluid obtained as above has been exploited for a quantitative study of hard and rare probes such as azimuthal jet anisotropy, nuclear modification factor of identified hadrons, disappearance of back-to-back jet correlation,  $J/\psi$  suppression, and direct photon emission [25].

#### B. Heavy quark diffusion in quark-gluon fluid

We solve the Langevin equation (1) and (2) with the drag coefficient  $\Gamma$  given by Eq. (12) in the local rest frame of the fluid element. The dimensionless parameter  $\gamma$  is inversely proportional to the relaxation time  $\tau_Q$  of a heavy quark as

$$\tau_Q = \frac{1}{\Gamma} = \frac{M_Q}{\gamma T^2}. \quad (17)$$

The  $\tau_Q$  is listed in Table I for three typical values,  $\gamma = 0.3$  (weak coupling),  $\gamma = 1.0$  (intermediate coupling), and  $\gamma = 3.0$  (strong coupling). The characteristic temperature felt by

TABLE I. Relaxation times of charm and bottom quarks for  $\gamma = 0.3, 1.0,$  and  $3.0$  at  $T = 210$  MeV.  $M_c$  and  $M_b$  are chosen to be  $1.5$  GeV and  $4.8$  GeV, respectively. (See also Table II.)

$\gamma$	0.30	1.0	3.0
$\tau_c$ (fm)	22	6.7	2.2
$\tau_b$ (fm)	72	21	7.2

TABLE II. Lifetimes of QGP for different centralities and freeze-out conditions. We adopt two characteristic impact parameters  $b = 3.1$  and  $5.5$  fm. (See also Table I.)

$f_0$	0	0.5	1
$\tau_{\text{QGP}}^{b=3.1\text{fm}}$ (fm)	9.8	5.9	4.5
$\tau_{\text{QGP}}^{b=5.5\text{fm}}$ (fm)	8.7	5.2	4.0

the heavy quark during the space-time history in the QGP fluid is taken to be  $210$  MeV (as for the reasoning of this number, see Sec. IV A1)

Let us now introduce an effective lifetime of QGP,  $\tau_{\text{QGP}}$ , by the following definition: At  $\tau = \tau_{\text{QGP}}$ , the QGP fraction  $f_{\text{QGP}}$  in Eq. (16) at  $x = y = z = 0$  reaches to  $f_0$ , which takes a value between 0 and 1. For  $f_0 = 0$ , the effective lifetime is defined as the time when QGP disappears completely, while  $f_0 = 1$  corresponds to the time when hadronic phase starts to appear. The effective lifetime of QGP is listed in Table II for two different impact parameters and for three different values of  $f_0$ .

From the comparison of  $\tau_Q$  and  $\tau_{\text{QGP}}$  in Tables I and II, one finds that the initial momentum distributions of charm and bottom quarks will be changed by QGP only slightly for the weak drag force ( $\gamma = 0.30$ ). However, for the strong drag force ( $\gamma = 3.0$ ), both charm and bottom quarks are affected by QGP and their momentum distributions would be modified substantially.

### 1. Initial distribution of heavy quarks

On the initial hypersurface  $\tau_0 = 0.6$  fm, initial transverse positions of heavy quarks are distributed according to the

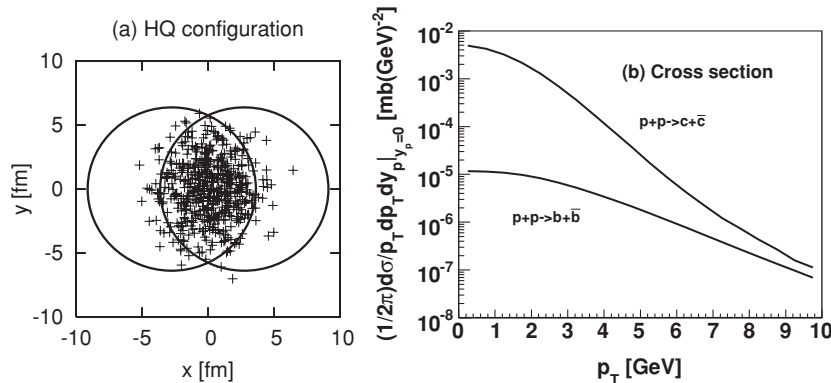


FIG. 1. (a) A sample of 500 heavy quarks at the initial in the transverse plane, for the Au + Au collision with impact parameter  $5.5$  fm. (b) Invariant cross sections of charm and bottom production in  $p + p$  collisions in midrapidity ( $|y_p| \leq 1.0$ ), which is proportional to the initial momentum distribution.

overlap function of two nuclei A and B in the transverse plane  $T_{\text{AB}}(x, y)$ :

$$T_{\text{AB}}(x, y) = T_A \left( x + \frac{b}{2}, y \right) T_B \left( x - \frac{b}{2}, y \right), \quad (18)$$

$$T_{\text{A(B)}}(x, y) = \int dz \rho_{\text{A(B)}}(x, y, z),$$

where  $\rho_{\text{A(B)}}$  is the Woods-Saxon parametrization of nuclear density. The heavy quarks are assumed to stream freely in the longitudinal direction for  $0 < \tau < \tau_0$  and acquire the momentum rapidity  $y_p = \eta_s$ . Thus the initial heavy quark distribution in the phase space reads

$$\frac{dN}{d^3 p d^2 x_\perp \tau_0 d\eta_s} = \frac{d\sigma_{pp}^{\text{HQ}}}{d^3 p} T_{\text{AB}}(x, y) \frac{\delta(\eta_s - y_p)}{\tau_0}. \quad (19)$$

The initial momentum spectrum of heavy quarks  $d\sigma_{pp}^{\text{HQ}}/d^3 p$  in  $p + p$  collisions is calculated by perturbative QCD to leading order (LO) using the event generator PYTHIA 6.4 [13].

In Fig. 1 the initial distribution of heavy quarks in the transverse plane and that in the momentum space at midrapidity ( $|y_p| \leq 1$ ) are shown. The momentum distribution is normalized to the invariant cross section in  $p + p$  collisions. Note that the initial momentum distribution of the charm quark has a steeper slope at high  $p_T$  than that of the bottom quark. Nuclear effects such as shadowing and Cronin effect are not considered for simplicity.

In Fig. 2(a), we show the differential cross section of electrons from heavy quarks in  $p + p$  collisions obtained by PYTHIA (the LO perturbative QCD). The theoretical cross section underestimates the experimental value by a factor 5–10 in magnitude as shown Fig. 2(b), while the shape of the cross section is reproduced well for  $p_T > 3$  GeV as shown in Figs. 2(a) and 2(b). The discrepancy is known to become smaller by taking into account higher orders beyond LO [26,27]. Because the  $p_T$  shape is more relevant than the magnitude in our study of  $R_{\text{AA}}$  and  $v_2$  for heavy quarks, we adopt LO for simplicity and compare our results with the data only above 3 GeV in the following.

### 2. Simulation of the Brownian motion

The Langevin equation of a heavy quark is defined in the local rest frame of QGP. The information of local flow velocity and local temperature at the position of the heavy quark is

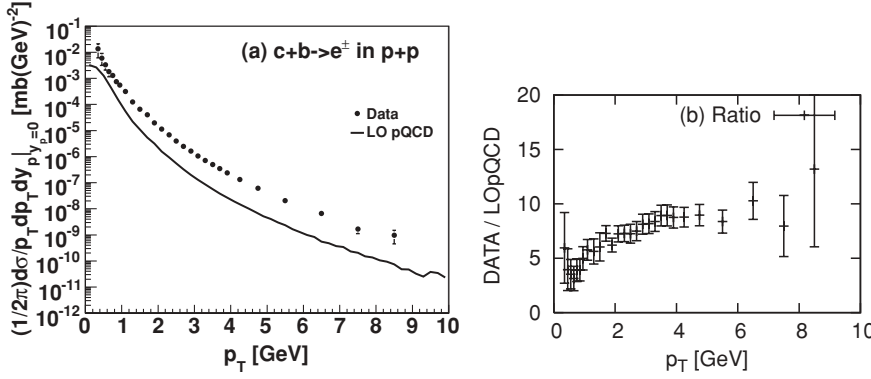


FIG. 2. (a) Experimental cross section for electron production in  $p + p$  collision at midrapidity [26] and the leading-order pQCD result by PYTHIA. (b) The ratio of the experimental data and the LO result. Theoretical calculations are performed at  $|y_p| \leq 0.35$  and then properly normalized to obtain the cross section.

supplied from the relativistic hydrodynamics. The algorithm of such Langevin simulation is summarized as follows:

- (i) Start from a sample of heavy quark at a position and a momentum according to the initial phase-space distribution given in Eq. (19).
- (ii) Given the phase-space location  $(p^\mu, x^\mu)$  in the laboratory frame, obtain the information of the local flow velocity  $u^\mu(x)$  and local temperature  $T(x)$  from the output of the hydrodynamic simulation.
- (iii-a) Coordinate step: Make one discrete step for the heavy quark in the configuration space according to Eq. (1) by using discrete proper-time step  $\Delta s = (M/E)\Delta t$ :

$$\Delta x^\nu(s) = \frac{P^\nu}{M} \Delta s. \quad (20)$$

- (iii-b) Momentum step: Move to the rest frame of the fluid element by the Lorentz transformation,  $p \rightarrow k$ . Make one discrete step for the heavy quark in momentum according to Eq. (2) using  $\Delta s$ :

$$\Delta \vec{k}(s) = -\gamma \frac{T^2 E(k)}{M^2} \vec{k} \Delta s + \vec{\xi}(s), \quad (21)$$

$$\langle \xi_i(s) \xi_j(s') \rangle = \delta_{ij} \delta_{ss'} \frac{2\gamma T^3}{M^2} E(E + T) \Delta s. \quad (22)$$

Then, move back to the laboratory frame by inverse Lorentz transformation ( $k + \Delta k \rightarrow p'$ ).

- (iv) Repeat the steps (ii) and (iii) until the volume fraction of QGP in the mixed phase ( $f_{\text{QGP}}$ ) reaches  $f_0$ .

Several comments are in order here about this procedure.

- (i) We use the proper time step  $\Delta s$  instead of the ordinary time step  $\Delta t$  in our simulation, simply because the former is a Lorentz scalar and thus easy to handle in going back and forth between the laboratory frame and the fluid rest frame. We choose  $\Delta s = 0.01$  fm in our simulation, which is much shorter than the relaxation time of the drag force parameter adopted in this article.
- (ii) Owing to the Itô discretization scheme, the momentum step in (iii-b) can be performed only by using the information of flow and temperature at the current position of the heavy quark in the phase space.
- (iii) It is not clear whether we should stop the heavy quark diffusion at the point when the mixed phase starts to appear or at the point when the mixed phase disappears. We consider this uncertainty as a systematic error and

consider the three cases as shown in Table II, namely  $f_0 = 0, 0.5, \text{ and } 1$ .

### 3. Freeze-out and decay

Once the local temperature around the charm(bottom) quark becomes lower than  $T_c$ , it hadronizes into  $D$  ( $B$ ) mesons. Because we need to calculate single-electron spectra from the heavy quarks, we focus on the following semileptonic decays:  $D \rightarrow e$  for  $D$  decay,  $B \rightarrow e$  for primary  $B$  decay, and  $B \rightarrow D \rightarrow e$  for secondary  $B$  decay. The hadronization of heavy quarks and the decay of heavy mesons are calculated by using PYTHIA 6.4 [13]. Because we employ independent fragmentation given by PYTHIA, the effect of quark recombination to form  $D$  or  $B$  mesons is not taken into account. Such simplification would be more reasonable for heavy quarks with higher transverse momentum. Therefore, it is the high- $p_T$  region (e.g., above 3 GeV) that is suitable to compare our results with the experimental data.

### C. Observables

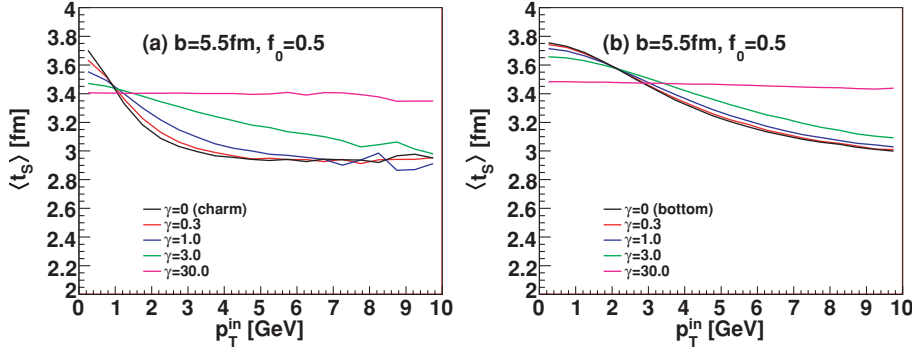
Medium modification factor  $R_{AA}$  for single electrons is defined by

$$R_{AA}(p_T) = \frac{1}{N_{\text{coll}}} \frac{dN_{A+A}/dp_T}{dN_{p+p}/dp_T}, \quad (23)$$

where  $N_{\text{coll}}$  is the number of binary collisions calculated from the Glauber model. Because the initial heavy quark distribution is assumed to be without nuclear effects and to scale as  $N_{\text{coll}}$  in our calculation, the deviation of  $R_{AA}$  from unity is solely attributed to the heavy quark diffusion in the hot medium. The elliptic flow for single electrons is defined by

$$v_2(p_T) = \frac{\int d\phi \frac{d^2 N_{A+A}}{dp_T d\phi} \cos 2\phi}{\int d\phi \frac{d^2 N_{A+A}}{dp_T d\phi}} = \langle \cos 2\phi \rangle. \quad (24)$$

This quantity indicates how much momentum anisotropy around the collision axis is given to the heavy quarks from the background medium.



#### IV. NUMERICAL RESULTS

Before showing the numerical results in detail, let us first summarize the basic parameters of our simulation. (1) The dimensionless drag coefficient  $\gamma$  is a parameter to control the diffusion of heavy quarks in QGP. We take three characteristic values,  $\gamma = 0.3, 1.0,$  and  $3.0$ , corresponding to weak, intermediate, and strong coupling, respectively. (2) The impact parameter  $b$  controls the volume and the lifetime of QGP. Thus it affects indirectly the heavy quark spectra at their freeze-out and the single-electron spectra. In all of the figures below except for Fig. 9,  $b$  is taken to be 5.5 fm (10–20% centrality). (3) The criterion of stopping the heavy quark diffusion in the mixed phase is given by  $f_0$  that takes a value between 0 and 1. Its dependence on the final results is considered to be a systematic error of our calculation. In all of the figures except for Fig. 9, we show the results at the central value,  $f_0 = 0.5$ .

##### A. Heavy quark spectra

###### 1. Profile of heavy quark diffusion

To estimate how long a heavy quark stays in the QGP region in terms of local fluid proper time, we define the “stay time” as

$$\begin{aligned} t_S &\equiv \sum_{\text{steps}} \Delta t|_{\text{FRF}} = \sum_{\text{steps}} \Delta s(E/M)|_{\text{FRF}} \\ &= \sum_{\text{steps}} \Delta s(p \cdot u/M)|_{\text{LF}}, \end{aligned} \quad (25)$$

where FRF and LF imply the fluid rest frame and laboratory frame, respectively. By averaging over the heavy quarks starting initially with  $p_T^{\text{in}}$  and ending in midrapidity ( $|y_p| \leq 1.0$ ) at their freeze-out, we obtain the average stay time  $\langle t_S \rangle$ .

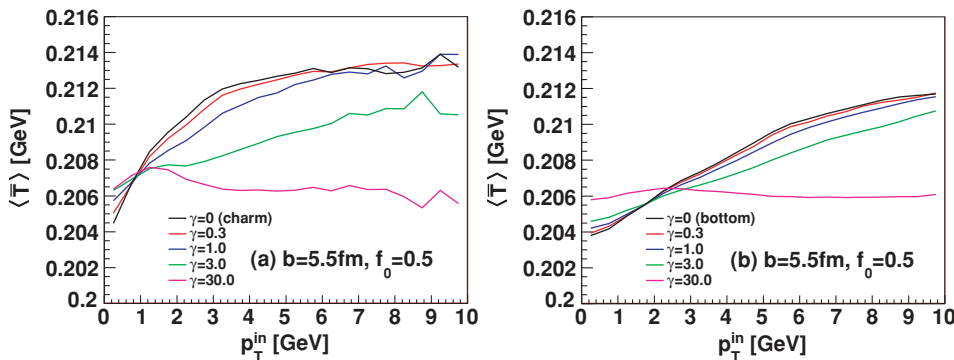


FIG. 3. (Color online) The averaged stay time  $\langle t_S \rangle$  of (a) charm quarks and (b) bottom quarks with the drag coefficient  $\gamma = 0, 0.3, 1.0, 3.0,$  and  $30.0$  at midrapidity ( $|y_p| \leq 1.0$ ). The impact parameter is chosen to be 5.5 fm in Au + Au collisions. For freeze-out condition,  $f_0 = 0.5$  is adopted.

Shown in Fig. 3 is the averaged stay time of heavy quarks as a function of their initial transverse momentum. The diffusion coefficient is taken to be  $\gamma = 0, 0.3, 1.0, 3.0,$  and  $30.0$ . Here  $\gamma = 0$  corresponds to the free streaming. However,  $\gamma = 30.0$  corresponds to the extremely strong coupling where the relaxation times at typical temperature 210 MeV are 0.22 fm for charm and 0.72 fm for bottom: The initial information on  $p_T$  is completely lost after a few fm of diffusion in this case.

The figure shows that, for heavy quarks with large initial velocity compared to the fluid velocity ( $p_T^{c,\text{in}} > 1 \text{ GeV}, p_T^{b,\text{in}} > 3 \text{ GeV}$ ), the stay time becomes shorter for higher  $p_T$  because they get out of the medium in shorter times. Also, as the drag force becomes stronger, the stay time becomes longer as expected. As for the heavy quarks with small initial velocity ( $p_T^{c,\text{in}} < 1 \text{ GeV}, p_T^{b,\text{in}} < 3 \text{ GeV}$ ), the stronger the drag force, the shorter the stay time, because the drag force from the background fluid accelerates them more strongly.

Next we define the averaged temperature for the heavy quarks experienced during their stay in the QGP fluid:

$$\bar{T} \equiv (1/t_S) \sum_{\text{steps}} T(x) \Delta t|_{\text{FRF}}. \quad (26)$$

By averaging over the heavy quarks starting initially with  $p_T^{\text{in}}$  and ending in midrapidity ( $|y_p| \leq 1.0$ ) at freeze-out, we obtain the averaged temperature  $\langle \bar{T} \rangle$  shown in Fig. 4.

The figure shows that, for heavy quarks with large initial velocity compared to the fluid velocity ( $p_T^{c,\text{in}} > 1 \text{ GeV}, p_T^{b,\text{in}} > 3 \text{ GeV}$ ), the averaged temperature becomes higher for higher  $p_T$  because they feel only the initial high temperature region before getting out of QGP. Also, as the drag force becomes stronger, the stay time becomes longer and averaged temperature becomes smaller. As for the heavy quarks with small initial

FIG. 4. (Color online) The averaged temperature  $\langle \bar{T} \rangle$  of (a) charm quarks and (b) bottom quarks with the drag coefficient  $\gamma = 0, 0.3, 1.0, 3.0,$  and  $30.0$  in midrapidity ( $|y_p| \leq 1.0$ ). The collision geometry and the freeze-out condition are the same with those in Fig. 3. The fluctuation in high  $p_T$  in (a) is due to statistical errors of our simulation.

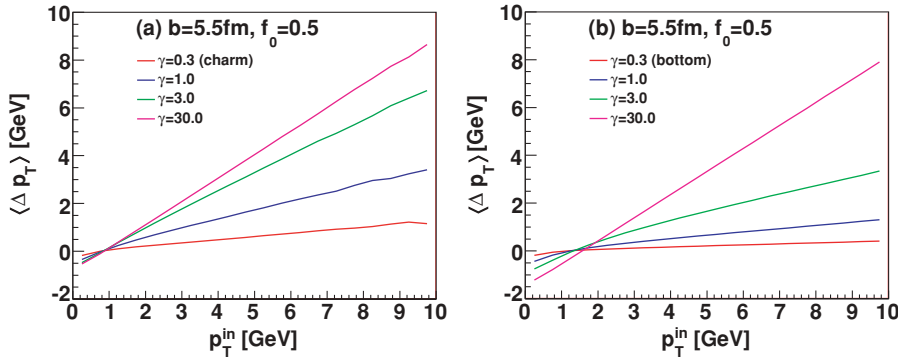


FIG. 5. (Color online) The averaged momentum loss  $\langle \Delta p_T \rangle$  of (a) charm quarks and (b) bottom quarks with drag coefficients  $\gamma = 0.3, 1.0, 3.0$ , and  $30.0$  in midrapidity ( $|y_p| \leq 1.0$ ). The collision geometry and the freeze-out condition are the same with those in Fig. 3.

velocity ( $p_T^{c,\text{in}} < 1$  GeV,  $p_T^{b,\text{in}} < 3$  GeV), the stronger the drag force, the higher the averaged temperature, because they are strongly accelerated and quickly pass the low temperature region. It turns out that the average temperature lies between 200 and 220 MeV in the wide range of  $p_T^{\text{in}}$  and  $\gamma$ ; this is the reason why we adopted the typical temperature 210 MeV in Sec. III.

Finally, let us define the the transverse momentum loss (momentum loss for short):

$$\Delta p_T = p_T^{\text{in}} - p_T^{\text{out}}, \quad (27)$$

where  $p_T^{\text{out}}$  is the transverse momentum at the time of the freeze-out of the heavy quark. By averaging over the heavy quarks starting initially with  $p_T^{\text{in}}$  and ending in midrapidity ( $|y_p| \leq 1.0$ ) at freeze-out, we obtain the averaged momentum loss  $\langle \Delta p_T \rangle$  as shown in Fig. 5.

For heavy quarks with larger initial  $p_T^{\text{in}}$ , the momentum loss per unit time (dynamical effect) is larger as seen in Eqs. (2) and (12) while the average stay time (kinematical effect) is shorter. Therefore, there are two competing effects in the net momentum loss: In Fig. 5, we find that larger initial momentum leads to larger momentum loss, so that the dynamical effect wins over the kinematical effect. As for the dependence on drag coefficient, both dynamical and kinematical effects act additively for heavy quarks with large initial momentum ( $p_T^{c,\text{in}} > 1$  GeV,  $p_T^{b,\text{in}} > 1.5$  GeV) and the momentum loss is enhanced by increasing  $\gamma$ . For the heavy quarks with small initial velocity ( $p_T^{c,\text{in}} < 1$  GeV,  $p_T^{b,\text{in}} < 1.5$  GeV), these two effects compete but we find in Fig. 5 that the dynamical effect seems to win, namely that the stronger the drag force, the larger the momentum gain by the acceleration from the fluid. Note here that, for the extreme case  $\gamma = 30.0$ , we have almost

a linear increase of  $\langle \Delta p_T \rangle = p_T^{\text{in}} - p_T^{\text{out}}$  as a function of  $p_T^{\text{in}}$ . This is simply because the heavy quarks are thermalized and  $p_T^{\text{out}}$  is almost independent of  $p_T^{\text{in}}$ .

## 2. Nuclear modification factor $R_{AA}^Q$

Let us define  $R_{AA}^Q$  ( $Q = c, b$ ) for heavy quarks by replacing the number of electrons  $N_{p+p}(N_{A+A})$  in Eq. (23) by the number of heavy quarks at the freeze-out  $N_{p+p}^Q$  ( $N_{A+A}^Q$ ). This is a theoretical quantity not directly accessible in experiment, but it is useful to examine the behavior of heavy quarks without the kinematical complication due to their semileptonic decays to electrons.

Shown in Fig. 6 are  $R_{AA}^Q$  for charm and bottom in the midrapidity at impact parameter 5.5 fm as a function of  $p_T^{\text{out}}$ . There are two key factors that determine  $R_{AA}^Q$ ; the momentum loss of heavy quarks and the initial distribution of heavy quarks. Starting from the initial distribution, the high-momentum quarks lose energy due to drag force and are shifted to the low  $p_T^{\text{out}}$  region. Therefore,  $R_{AA}^Q$  is suppressed (enhanced) at high (low)  $p_T^{\text{out}}$ . This tendency is prominent for large drag force as expected. Also, the suppression at high  $p_T^{\text{out}}$  is larger for the charm if we adopt the same  $\gamma$ . This is because the actual drag coefficient is  $\gamma T^2/M_Q$  so that the quark with smaller mass is affected more by the drag force.

## 3. Elliptic flow $v_2^Q$

In Fig. 7, we show the elliptic flow for the heavy quark  $v_2^Q$  ( $Q = c, b$ ) at midrapidity at impact parameter 5.5 fm. It is clear that the charm and bottom quarks with any drag force at large  $p_T^{\text{out}}$  are less thermalized and thus they do not

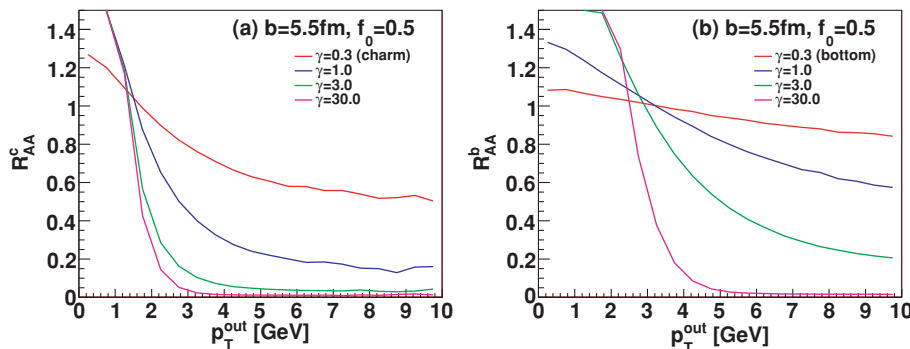


FIG. 6. (Color online)  $R_{AA}^Q$  of (a) charm quarks and (b) bottom quarks with drag coefficients  $\gamma = 0.3, 1.0, 3.0$ , and  $30.0$  at midrapidity ( $|y_p| \leq 1.0$ ). For collision geometry, we choose the impact parameter 5.5 fm in Au + Au collisions. For freeze-out condition, the  $f_0 = 0.5$  is adopted.

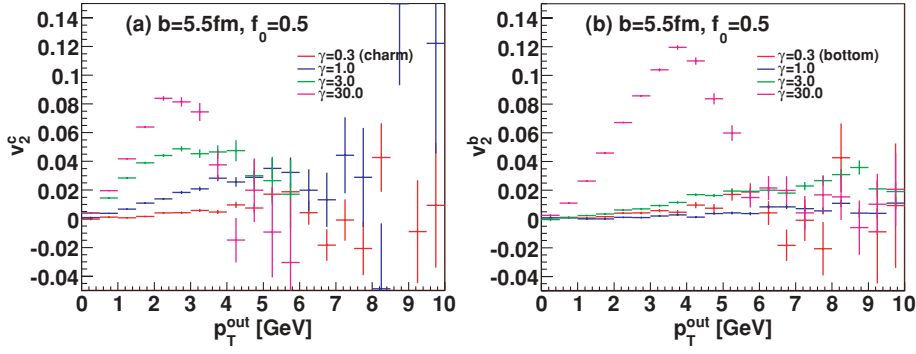


FIG. 7. (Color online)  $v_2^Q$  of (a) charm quarks and (b) bottom quarks with drag coefficients  $\gamma = 0.3, 1.0, 3.0,$  and  $30.0$  in midrapidity ( $|y_p| \leq 1.0$ ). The collision geometry and the freeze-out condition are the same with those in Fig. 6. In (a), the statistical errors for  $\gamma = 3.0$  and  $30.0$  are so large at  $p_T^{\text{out}} > 6$  GeV that we omit them.

produce much momentum anisotropy. Note that the dominant contributions of heavy quarks with  $\gamma = 30.0$  at large  $p_T^{\text{out}}$  may be those that start outside of the QGP fireball and with large initial  $p_T^{\text{in}}$ , therefore they have isotropic momentum distribution because there is no medium effect [28]. However, charm quarks with small  $p_T^{\text{out}}$  are thermalized for large drag force and develops  $v_2^Q$  reflecting the flow of light particles. As for bottom quarks, they only have small momentum anisotropy with all drag forces but  $\gamma = 30.0$  at small  $p_T^{\text{out}}$  because they are not enough thermalized.

## B. Electron spectra

### 1. Nuclear modification factor $R_{AA}$

Let us now examine the results of electrons and positrons (we call them just electrons for short) that are the decay products from  $D$  and/or  $B$  mesons. In Figs. 8(a), 8(b), and 8(c), we show  $R_{AA}$  of electrons (a) from charm quarks, (b) from bottom quarks, and (c) from charm+bottom quarks. The dependence of  $R_{AA}$  on the drag coefficient  $\gamma$  is understood

easily: Larger drag coefficient gives larger energy loss and  $R_{AA}$  is suppressed. There is, however, one qualitative difference between  $R_{AA}^Q$  in Sec. IV A 2 and  $R_{AA}$  in the low- $p_T$  region:  $R_{AA}^Q$  exceeds unity due to the shift of the high-momentum quarks to low-momentum quarks, while  $R_{AA}$  stays around unity at low momentum. This is understood by recognizing that the low- $p_T$  electrons come from a wide range of heavy quarks with various freeze-out momenta, so low-momentum electrons are not sensitive to the modification of the heavy quark spectrum due to diffusion. However, the electrons with high  $p_T$  originate mainly from high- $p_T$  heavy quarks and thus they are sensitive to the spectral change of heavy quarks.

In Fig. 8(d), the number of electrons from bottom divided by that from charm + bottom for Au + Au collision is shown as a function of electron's  $p_T$  together with that for  $p + p$  collision. In both  $p + p$  and  $A + A$ , more than 50% of electrons come from the bottom for  $p_T > 3$  GeV. Furthermore, the ratio increases as the drag force becomes stronger. The kink structure of  $R_{AA}$  at  $p_T \sim 1-2$  GeV in Fig. 8(c) is understood by

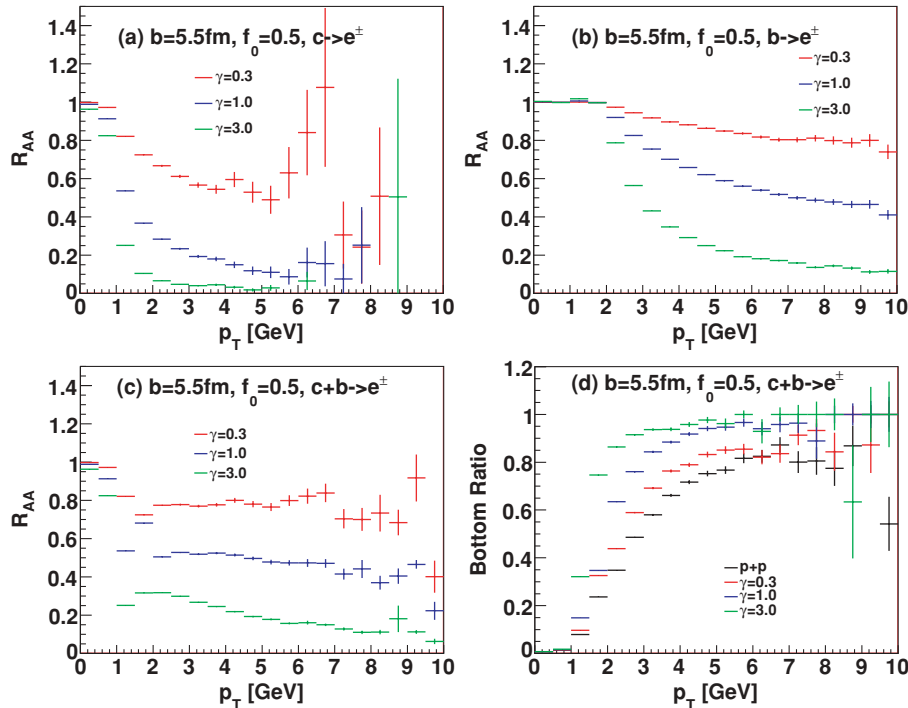


FIG. 8. (Color online) (a)  $R_{AA}$  of electrons from charm, (b)  $R_{AA}$  of electrons from bottom, (c)  $R_{AA}$  of electrons from both charm and bottom, and (d) the ratio of electrons from the bottom and the net electrons. All results are in midrapidity ( $|y_p| \leq 0.35$ ). The drag coefficient is taken to be  $\gamma = 0.3, 1.0,$  and  $3.0$ . The impact parameter is taken to be  $5.5$  fm in Au + Au collisions. For freeze-out condition, the  $f_0 = 0.5$  is adopted. In (d), the result of  $p + p$  collision calculated in the leading-order pQCD by PYTHIA is also plotted.

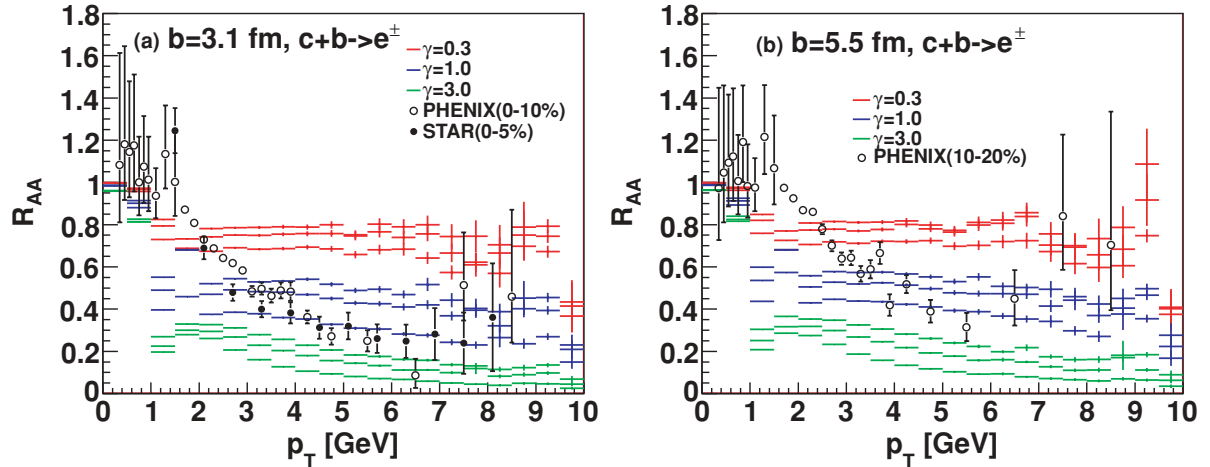


FIG. 9. (Color online) Comparison of  $R_{AA}$  in our hydro + heavy-quark model with the experimental data [4,5]. The Au + Au collision with the impact parameter (a) 3.1 fm and (b) 5.5 fm, both in midrapidity,  $|y_p| \leq 0.35$ . The drag coefficient is chosen to be  $\gamma = 0.3, 1.0,$  and  $3.0$  indicated by different colors. The freeze-out condition is taken to be  $f_0 = 1.0, 0.5,$  and  $0.0$  which correspond to upper, middle, and lower points, respectively, within the same color. As for error bars in experimental data, we only plot the statistical errors [4,5].

the fact that the dominant contribution to the electrons changes rapidly from the charm to the bottom.

Finally we compare our numerical results with experimental data [4] in Fig. 9. Here we show two cases of impact parameters 3.1 fm (0–10% centrality) and 5.5 fm (10–20% centrality) at midrapidity. The systematic errors due to the freeze-out condition of heavy quarks are represented by the three plots with the same color. Recall that the comparison of our results and experimental data is reliable only for  $p_T > 3$  GeV as discussed in Sec. III B1 and that bottom quarks are the dominant source of electrons in this region.

Although definite conclusion cannot be made from the present comparison, it is likely that the intermediate to large value of the drag coefficient  $\gamma = 1.0$ – $3.0$  is favored especially for small impact parameter. This number is rather close to

the value  $\gamma = 2.1 \pm 0.5$  predicted from the AdS/CFT correspondence [see Eq. (11)]. We should remark, however, that the radiative energy loss [7,18] and the relativistic diffusion via resonances combined with quark coalescence [17] would be legitimate alternatives to describe the data, so further systematic comparison of the data and theoretical calculations is called for.

## 2. Elliptic flow $v_2$

We show our theoretical  $v_2$  of electrons in Fig. 10 as a function of  $p_T$  together with the experimental data [4]. Our  $v_2$  does not depend much on the strength of the drag force for  $p_T > 3$  GeV and stays small. Due to the poor statistic of both our simulation and the experimental data in the relevant region, it is not clear whether theory and experiment are consistent with each other. Although it is still preliminary, recent PHENIX data show large  $v_2 = 0.05$ – $0.1$  with small errors for  $3 < p_T < 5$  GeV at collisions with corresponding centrality [29].

## V. SUMMARY AND CONCLUDING REMARKS

In this article, we have examined the diffusion of heavy quarks in the dynamical QGP fluid on the basis of the relativistic Langevin equation combined with the relativistic hydrodynamics. We establish a generalized fluctuation-dissipation relation in Itô discretization scheme, Eq. (7), which relates the diffusion constant  $D(p)$  and the drag coefficient  $\Gamma(p)$  for the relativistic Brownian particle. Then we parametrized the drag coefficient motivated by the formula from the AdS/CFT correspondence for strongly coupled plasma,  $\Gamma \equiv \gamma T^2/M$ , with the dimensionless coefficient  $\gamma$  as a parameter. The space-time evolution of the QGP fluid composed of light quarks and gluons is treated by the full

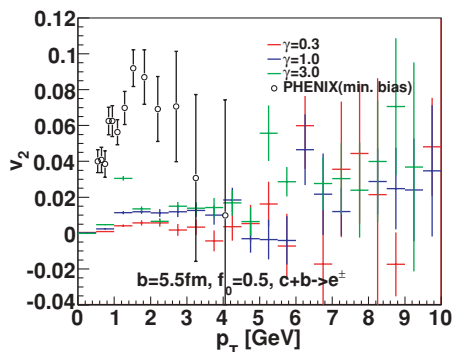


FIG. 10. (Color online) Comparison of  $v_2$  in our hydro + heavy-quark model with experimental data [4] in midrapidity ( $|y_p| \leq 0.35$ ). Experimental data of  $v_2$  is obtained in minimum bias analysis, whereas our theoretical values of  $v_2$  are evaluated at impact parameter 5.5 fm as a representative. The drag coefficient is chosen to be  $\gamma = 0.3, 1.0,$  and  $3.0$  and the freeze-out condition is  $f_0 = 0.5$ . As for error bars in experimental data, we only plot the statistical errors [4].

(3+1)-dimensional relativistic hydrodynamics for the perfect fluid.

By solving the Langevin equation for heavy quarks under the influence of the QGP fluid, we obtain the space-time history of the diffusion process of charm and bottom in the realistic situation of the relativistic heavy-ion collisions. The initial momentum distributions of charm/bottom are given by the event generator PYTHIA. The hadronization and the semileptonic decays of charm/bottom after they leave from the QGP region are treated by independent fragmentation and decay. Nuclear effects for initial charm/bottom distributions and the quark recombination/coalescence in hadronization of heavy quarks, which would be important for the low  $p_T < 3$  GeV region of the final electron spectrum, are neglected for simplicity in this article.

Because we have the space-time history of the charm/bottom during their diffusion, we have looked at the average stay time of heavy quarks in QGP  $\langle t_S \rangle$ , the average temperature felt by heavy quarks in QGP  $\langle \bar{T} \rangle$ , and the average momentum loss  $\langle \Delta p \rangle$  during the diffusion. We have also looked at the nuclear modification factor  $R_{AA}^Q$  and the elliptic flow  $v_2^Q$  of heavy quarks as a function of the transverse momentum of the heavy quarks at their freeze-out  $p_T^{\text{out}}$ . The results indicate that, for sufficiently large values of  $p_T^{\text{out}} > 3$  GeV, there is a sizable suppression of  $R_{AA}^Q$  for large drag coefficient, while one can see only a significant effect in  $v_2^Q$  only for  $p_T^{\text{out}} < 3$  GeV that is not the region one can rely on our calculation.

We then compared our calculations of  $R_{AA}$  and the elliptic flow  $v_2$  for single electron with the RHIC data. First, the momentum distribution of the electrons do not necessarily reflect the shape of the momentum distribution of the heavy quarks at their freeze-out due to decay kinematics. Also, the net electrons with  $p_T > 3$  GeV are dominated by those from bottom quarks. A rough comparison of  $R_{AA}$  for  $p_T > 3$  GeV suggests that the drag coefficient could be as large as  $\gamma = 1.0$ – $3.0$ . However, we are unable to extract useful information from  $v_2$  for  $p_T > 3$  GeV because of the lack of statistics in both experiment and simulations. The value of  $\gamma = 1.0$ – $3.0$  is consistent with that predicted by the AdS/CFT approach for strongly interacting plasma ( $\gamma = 2.1 \pm 0.5$ ), although we could not exclude other descriptions of heavy quarks in QGP such as radiative stopping [7,18] and the resonance scattering model [17]. High-precision experimental data at RHIC and LHC for electrons from charm and bottom identified separately are highly desirable. Also the correlation of the transverse momenta of a heavy quark and a heavy antiquark (and the associated electron-positron or  $D$ - $\bar{D}$  correlation [30,31]) could be a good observable to make detailed comparison of the theories and experiments.

Before closing, we remark on possible improvements of our approach to treat the region  $p_T < 3$  GeV in a more reliable way: (i) Initial heavy quark distributions beyond LO need to be considered for better control of their absolute magnitude, the  $p_T$  shape, and the charm/bottom ratio, (ii) nuclear effects on the initial charm/bottom distribution need to be examined, and (iii) the hadronization of charm/bottom due to quark recombination processes needs to be taken into account.

## ACKNOWLEDGMENTS

Part of this work was carried out during Y. Akamatsu's visit to the European Centre for Theoretical Studies in Nuclear Physics and Related Areas (ECT\*). Y.A. thanks ECT\* and J. P. Blaizot for their kind hospitality. The authors thank Tetsuo Matsui for fruitful discussions. Y.A. is supported by JSPS grants for Young Scientists. T. Hatsuda and T. Hirano are supported in part by the Grants-in-Aid of the Japanese Ministry of Education, Culture, Sports, Science and Technology (Nos. 18540253 and 19740130). T. Hirano is also supported by Sumitomo Foundation No. 080734.

## APPENDIX: RELATIVISTIC KRAMERS EQUATION

In this Appendix, we derive the partial differential equation of  $P(\vec{p}, \vec{x}, t)$  or the Kramers equation using the Itô (prepoint) discretization scheme. We give here the general form of the relativistic Langevin equation as

$$\begin{aligned} d\vec{x}(t) &= \frac{p(\vec{t})}{E(p(\vec{t}))} \Delta t, \\ d\vec{p}(t) &= -A(p(\vec{t}))\vec{p}(\vec{t})\Delta t + \sqrt{B(p(\vec{t}))}\vec{\eta}(t)\Delta t, \\ W[\vec{\eta}(t)]d^3\eta(t) &= C \cdot \exp\left[-\frac{\Delta t}{2}\vec{\eta}(t)^2\right]d^3\eta(t), \\ \langle \eta_i(t)\eta_j(t') \rangle &= \frac{\delta_{ij}\delta_{tt'}}{\Delta t}, \end{aligned} \quad (\text{A1})$$

where  $E(p) = \sqrt{\vec{p}^2 + M^2}$  with  $M$  being the mass of the Brownian particle. Here  $\vec{t} \equiv t$  corresponds to the Itô discretization and  $\vec{t} \equiv t + \Delta t$  corresponds to the Hanggi-Klimontovic discretization [15]. Also  $A(p)$ ,  $B(p)$ , and  $\vec{\eta}(t)$  in the Itô discretization correspond to  $\Gamma(p)$ ,  $D(p)$ , and  $\xi(t)/(\sqrt{D(p)}\Delta t)$  in the text, respectively. Because the Langevin equation is based on Markovian process, one needs information only at time  $t'$  to know the probability at later time  $t$ :

$$\begin{aligned} P(\vec{p}, \vec{x}, t | \vec{p}_0, \vec{x}_0, t_0) \\ = \int d^3p' d^3x' P(\vec{p}, \vec{x}, t | \vec{p}', \vec{x}', t') P(\vec{p}', \vec{x}', t' | \vec{p}_0, \vec{x}_0, t_0), \end{aligned} \quad (\text{A2})$$

where  $P(X, t | X_0, t_0)$  ( $X = \{\vec{p}, \vec{x}\}$ ) represents the conditional distribution function with a fixed initial condition  $X_0$  at time  $t_0$ . To derive the partial differential equation, we have to calculate  $P(X, t + \Delta t | X', t)$  from the Langevin equation. From the definition of  $P(X, t + \Delta t | X', t)$ ,

$$\begin{aligned} P(X, t + \Delta t | X', t) &\equiv \langle \delta(X - X(t + \Delta t)) \rangle_{t, X'} \\ &= \langle \delta[X - X' - \Delta X(\eta(t), t)] \rangle \\ &= \sum_{m=0}^{\infty} \langle [-\Delta X(\eta(t), t)]^m \rangle \frac{1}{m!} \partial_X^m \delta(X - X'), \\ \langle Y(\eta(t), t) \rangle &\equiv \int d^3\eta(t) W[\eta(t)] Y(\eta(t), t). \end{aligned} \quad (\text{A3})$$

Here  $\langle \dots \rangle_{t, X'}$  in the first line of Eq. (A3) represents the conditional probability with the fixed initial condition  $X(t) = X'$ . Note that in the last line of Eq. (A3), the average is expressed by the variables at time  $t$ . Inserting Eq. (A3) into

Eq. (A2), we obtain

$$\begin{aligned}
& P(X, t + \Delta t | X_0, t_0) \\
&= \int dX' P(X, t + \Delta t | X', t) P(X', t | X_0, t_0) \\
&= \int dX' \left[ \delta(X - X') + \sum_{m=1}^{\infty} \langle [-\Delta X(\eta(t), t)]^m \rangle \right. \\
&\quad \left. \times \frac{1}{m!} \partial_X^m \delta(X - X') \right] \cdot P(X', t | X_0, t_0) \\
&= P(X, t | X_0, t_0) \\
&\quad + \sum_{m=1}^{\infty} \frac{1}{m!} \partial_X^m \langle [-\Delta X(\eta(t), t)]^m \rangle P(X, t | X_0, t_0) \\
&= P(X, t | X_0, t_0) + \Delta t \partial_t P(X, t | X_0, t_0). \tag{A4}
\end{aligned}$$

In the Itô discretization scheme, the relevant average values  $\langle [\Delta X(\eta(t), t)]^m \rangle$  are

$$\begin{aligned}
\langle \Delta \vec{x}(t) \rangle &= \frac{\vec{p}(t)}{E(p(t))} \Delta t, \\
\langle \Delta \vec{p}(t) \rangle &= -A(p(t)) \vec{p}(t) \Delta t, \tag{A5} \\
\langle \Delta p_i(t) \Delta p_j(t) \rangle &= B(p(t)) \delta_{ij} \Delta t,
\end{aligned}$$

and the others are in higher order in  $\Delta t$ .

From Eqs. (A4) and (A5), the resulting relativistic Kramers equation reads

$$\begin{aligned}
& \left( \frac{\partial}{\partial t} + \frac{\vec{p}}{E} \frac{\partial}{\partial \vec{x}} \right) P(\vec{p}, \vec{x}, t) \\
&= \frac{\partial}{\partial \vec{p}} \left( A(p) \vec{p} + \frac{1}{2} \frac{\partial}{\partial \vec{p}} B(p) \right) P(\vec{p}, \vec{x}, t). \tag{A6}
\end{aligned}$$

- 
- [1] K. Yagi, T. Hatsuda, and Y. Miake, *Quark-Gluon Plasma* (Cambridge University Press, Cambridge, 2005); *Proceedings of Quark Matter 2008*, J. Phys. G: Nucl. Part. Phys. **35**, (2008).
- [2] T. Hirano, N. van der Kolk, and A. Bilandzic, arXiv:0808.2684 [nucl-th].
- [3] A. Vitev, J. Phys. G: Nucl. Part. Phys. **35**, 104011 (2008).
- [4] A. Adare *et al.* (PHENIX Collaboration), Phys. Rev. Lett. **98**, 172301 (2007).
- [5] B. I. Abelev *et al.* (STAR Collaboration), Phys. Rev. Lett. **98**, 192301 (2007).
- [6] M. Djordjevic, J. Phys. G: Nucl. Part. Phys. **32**, S333 (2006).
- [7] S. Wicks, W. Horowitz, M. Djordjevic, and M. Gyulassy, Nucl. Phys. A **784**, 426 (2007).
- [8] S. Caron-Huot and G. D. Moore, Phys. Rev. Lett. **100**, 052301 (2008); J. High Energy Phys. 02 (2008) 081.
- [9] S. S. Gubser, Phys. Rev. D **74**, 126005 (2006).
- [10] J. Casalderrey-Solana and D. Teaney, Phys. Rev. D **74**, 085012 (2006).
- [11] C. P. Herzog, A. Karch, P. Kovtun, C. Kozcaz, and L. G. Yaffe, J. High Energy Phys. 07 (2006) 013.
- [12] S. S. Gubser, Phys. Rev. D **76**, 126003 (2007).
- [13] T. Sjostrand, S. Mrenna, and P. Skands, J. High Energy Phys. 05 (2006) 026.
- [14] P. Langevin, C. R. Acad. Sci. Paris **146**, 530 (1908); N. G. Van Kampen, *Stochastic Processes in Physics and Chemistry* (North-Holland, Amsterdam, 2007).
- [15] F. Debbasch, K. Mallick, and J. P. Rivet, J. Stat. Phys. **88**, 945 (1997); F. Debbasch and J. P. Rivet, J. Stat. Phys. **90**, 1179 (1998); C. Chevalier and F. Debbasch, J. Math. Phys. **49**, 043303 (2008). For general discussions on momentum-dependent diffusion constant, see, P. Arnold, Phys. Rev. E **61**, 6091 (2000).
- [16] G. D. Moore and D. Teaney, Phys. Rev. C **71**, 064904 (2005).
- [17] H. van Hees and R. Rapp, Phys. Rev. C **71**, 034907 (2005). See also, R. Rapp and H. van Hees, arXiv:0803.0901 [hep-ph] and references therein.
- [18] N. Armesto, M. Cacciari, A. Dainese, C. A. Salgado, and U. A. Wiedemann, Phys. Lett. **B637**, 362 (2006).
- [19] T. Hirano, U. Heinz, D. Kharzeev, R. Lacey, and Y. Nara, Phys. Lett. **B636**, 299 (2006).
- [20] T. Hirano, Phys. Rev. C **65**, 011901(R) (2001).
- [21] T. Hirano and K. Tsuda, Phys. Rev. C **66**, 054905 (2002).
- [22] Recent lattice QCD simulations with (2+1)-flavor dynamical quarks suggest crossover for the transition between the hadronic phase and the quark-gluon plasma at zero chemical potential [23]. In this article, however, the bag equation of state, which shows the first-order phase transition, is employed for simplicity.
- [23] Y. Aoki, G. Endrodi, Z. Fodor, S. D. Katz, and K. K. Szabo, Nature (London) **443**, 675 (2006).
- [24] J. D. Bjorken, Phys. Rev. D **27**, 140 (1983).
- [25] T. Hirano and Y. Nara, Phys. Rev. C **68**, 064902 (2003); **69**, 034908 (2004); Phys. Rev. Lett. **91**, 082301 (2003); M. Isse, T. Hirano, R. Mizukawa, A. Ohnishi, K. Yoshino, and Y. Nara, Int. J. Mod. Phys. E **16**, 2338 (2007); T. Gunji, H. Hamagaki, T. Hatsuda, and T. Hirano, Phys. Rev. C **76**, 051901(R) (2007); F.-M. Liu, T. Hirano, K. Werner, and Y. Zhu, Phys. Rev. C **79**, 014905 (2009).
- [26] A. Adare *et al.* (PHENIX Collaboration), Phys. Rev. Lett. **97**, 252002 (2006).
- [27] M. Cacciari, P. Nason, and R. Vogt, Phys. Rev. Lett. **95**, 122001 (2005).
- [28] Our model assumes instantaneous hadronization and semileptonic decay once the freeze-out condition is satisfied. Heavy quarks starting outside and crossing the QGP fireball remain to be investigated.
- [29] D. Hornback, J. Phys. G: Nucl. Part. Phys. **35**, 104113 (2008).
- [30] X. Zhu, M. Bleicher, S. L. Huang, K. Schweda, H. Stoecker, N. Xu, and P. Zhuang, Phys. Lett. **B647**, 366 (2007).
- [31] X. Zhu, N. Xu, and P. Zhuang, Phys. Rev. Lett. **100**, 152301 (2008).